

Article

Unidirectional Invisibility in PT-Symmetric Cantor Photonic Crystals

Min Wu ¹, Fangmei Liu ², Dong Zhao ² and Yang Wang ^{2,*}

¹ School of Mathematics and Statistics, Hubei University of Science and Technology, Xianning 437100, China; wumin@hbust.edu.cn

² School of Electronic and Information Engineering, Hubei University of Science and Technology, Xianning 437100, China; liufangmei@hbust.edu.cn (F.L.); zhaodong@hbust.edu.cn (D.Z.)

* Correspondence: wangyang@hbust.edu.cn

Abstract: In this paper, we investigate the nonreciprocity of reflection in parity-time–symmetric (PT-symmetric) Cantor photonic crystals (PCs). Two one-dimensional PCs abiding by the Cantor sequence are PT-symmetric about the center. The PT symmetry and defect cavities in Cantor PCs can induce optical fractal states which are transmission modes. Subsequently, the left and right reflectionless states are located on both sides of a transmission peak. The invisible effect depends on the incident direction and the invisible wavelength can be modulated by the gain–loss factor. This study has potential applications in tunable optical reflectors and invisible cloaks.

Keywords: Cantor sequence; unidirectional invisibility; reflectionless photonic crystal; PT symmetry



Citation: Wu, M.; Liu, F.; Zhao, D.; Wang, Y. Unidirectional Invisibility in PT-Symmetric Cantor Photonic Crystals. *Crystals* **2022**, *12*, 199. <https://doi.org/10.3390/cryst12020199>

Academic Editor: Alessandro Chiasera

Received: 29 December 2021

Accepted: 26 January 2022

Published: 28 January 2022

Publisher's Note: MDPI stays neutral with regard to jurisdictional claims in published maps and institutional affiliations.



Copyright: © 2022 by the authors. Licensee MDPI, Basel, Switzerland. This article is an open access article distributed under the terms and conditions of the Creative Commons Attribution (CC BY) license (<https://creativecommons.org/licenses/by/4.0/>).

1. Introduction

Optical invisibility has been extensively utilized for sensors, filters, and other civilian facilities [1–3]. The traditional stealth technology is based on the ability of invisibility cloaks' materials to absorb light wave energy [4,5], but specific materials can only absorb light waves with specific wavelengths. Therefore, once the probing wavelength changes, the stealth effect will be greatly reduced. In addition, it is generally difficult for the absorption rate of light wave energy to reach a hundred percent [6] as there is energy surplus reflected by objects, meaning that it is necessary to find a new optical structure to realize the stealth of light waves and achieve a flexible adjustment to the stealth wavelength.

Optical systems are non-Hermitian, as there is gain or loss (or both of them) in the dielectrics [7]. Exchanges of energy occur between non-Hermitian optical systems and the outside world [8,9]. The dielectric refractive index in non-Hermitian can be written as $n = n_r + i*n_i$, where n_r is the real part of the refractive index, n_i is the imaginary part of the refractive index, and the letter i represents the imaginary unit.

As a non-Hermitian optical system satisfies parity-time (PT) symmetry, the left and right incident light waves are non-reciprocal [10]. Specifically, the left and right reflection spectra do not coincide. The two reflection coefficients' phase spectra curves are also not coincident [11]. The conception of PT symmetry is first derived from quantum mechanics [12]. In an optical system, as long as the refractive index of the dielectric meets the condition of $n(r) = n^*(-r)$ in space, where r is the position coordinate, the structure is PT-symmetric. Many fascinating physical phenomena have been observed in PT-symmetric and non-Hermitian systems, such as coherent perfect absorbing [13,14], optical bistability [15,16], optical solitons [17], optical gradient forces [18], and topological protected or transmission modes [19–22].

There are some defect modes in defective photonic crystals, such as one of the transmission modes [23]. The transmission mode has great value in transmittance and a very low reflectivity. The PT-symmetric optical system can enhance the resonance of the defect mode, so that the maximum transmittance does not coincide with the left and right zero

points of reflection [24]. In other words, the two reflectionless points are not coincident. This effect is called the unidirectional invisibility of optical propagation. Furthermore, the left and right reflectivity zero points, *viz.* the invisibility wavelength, can be regulated by the imaginary part of the dielectric refractive index [25].

Compared with periodic photonic crystals, quasi-periodic photonic crystals have more defect cavities and show the optical fractal effect [26,27]. The optical fractal states are transmission modes. Therefore, one can consider combining PT symmetry and quasi-periodic photonic crystals to achieve the optical unidirectional invisibility of particular wavelengths, using the reflection reciprocity of the left and right incident light waves around the optical fractal states. The optical fractal states are between the left and right reflectionless points in the reflection spectra. The stealth wavelength may also be adjusted flexibly by the imaginary refractive index of the dielectrics.

A centrosymmetric composite system was constructed from two quasi-photonic crystals which submit to the Cantor sequence. We modulated the gain–loss factor in systems to satisfy PT symmetry. An optical fractal state and the mode enhancement phenomenon of light were demonstrated subsequently. Then, we showed the nonreciprocity of reflection for incident light from the left and right, respectively. Next, the left and right zero point trajectories of reflection are given in the parameter space of the gain–loss factor and the normalized frequency. The dependence of invisible wavelength on the gain–loss factor was studied as well. Finally, we show the left/right reflectance changing with the gain–loss factor, as the incident wavelength is equal to the right/left reflectionless wavelength. This study may be utilized for optical invisibility.

2. PT-Symmetric Cantor Photonic Crystal

The Cantor sequence submits to the substitution rule: $S_0 = H, S_1 = HLH, S_2 = HLHLLLHLH, \dots, S_N = S_{N-1} (LLL)^{N-1} S_{N-1}, \dots$, where $N (N = 2, 3, \dots)$ is the sequence number, and S_N represents the N th term of the sequence [28].

Figure 1 gives a parity-time-symmetric (PT-symmetric) Cantor photonic crystal with a sequence number of $N = 2$. The S_2 Cantor photonic crystal can be expressed as HLHLLLHLH, where H and L represent two unique dielectric slabs with high and low refractive indices, respectively. The two dielectrics of H and L arrange along the Z-axis to form two S_2 Cantor photonic crystals which are centrosymmetric about the origin. Then, the imaginary part of dielectric refractive index is modulated to satisfy PT symmetry. The whole system can also be denoted by HLHLLLHLHH'L'H'L'L'H'L'H'.

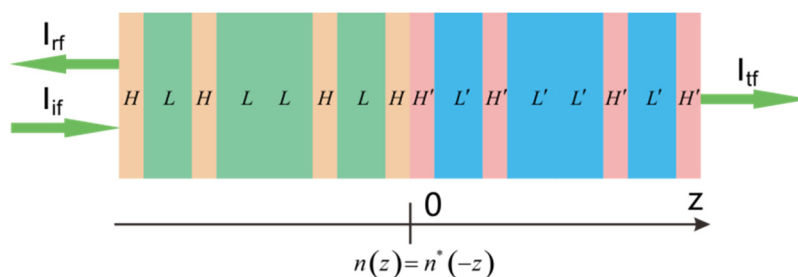


Figure 1. Schematic of PT-symmetric Cantor photonic crystal. The Cantor photonic crystal is composed of two S_2 dielectric multilayers submitted to the Cantor sequence substitution rule and the two S_2 of Cantor photonic crystal are symmetric about the center.

For a light incident from the left, the symbols of I_{if} , I_{tf} , and I_{rf} represent the incident, transmitted, and reflected lights, respectively, while for a right incident light beam the incident, transmitted, and reflected lights are, respectively, denoted by I_{ib} , I_{tb} , and I_{rb} . The alphabet of θ is the incident angle and for a normal incident beam the incident angle is $\theta = 0^\circ$.

The host materials of dielectric slabs H and H' are Si and have relatively high refractive indices. Their refractive indices are, respectively, expressed as $n_H = 3.53 + i \times 0.01 q$ and

$n_{H'} = 3.53 - i \cdot 0.01 q$, where i is the imaginary unit and q is the gain–loss factor of materials. The host materials of the low refractive indices dielectric slabs L and L' are SiO₂, of which the refractive indices are written as $n_L = 1.46 + i \cdot 0.01 q$ and $n_{L'} = 1.46 - i \cdot 0.01 q$, respectively. The thicknesses of dielectric slabs of H and H' are 1/4 optical wavelength, *viz.* $d_H = d_{H'} = \lambda_0/4/\text{Re}(n_H) = 0.1098 \mu\text{m}$, where $\lambda_0 = 1.55 \mu\text{m}$ is the central wavelength and $\text{Re}(n_H)$ is the real part of n_H . Similarly, the thicknesses of dielectric slabs of L and L' are $d_L = d_{L'} = \lambda_0/4/\text{Re}(n_L) = 0.2654 \mu\text{m}$. The PT symmetry requires the system refractive index to meet the condition of $n(z) = n^*(-z)$, and the asterisk represents the complex conjugate operator. If we further write the system refractive index as $n(z) = n_r(z) + i \cdot n_i(z)$, the PT-symmetric condition can be divided into two formulae: $n_r(z) = n_r(-z)$ and $n_i(z) = -n_i(-z)$. That is, the real part of the refractive index is even symmetric with respect to the origin, while the imaginary part is odd symmetric. Otherwise, the positive imaginary part of the refractive index represents the optical loss in materials, while the negative value of the refractive index indicates the optical gain. One can realize optical gain by nonlinear two-wave mixing and the loss could be modulated through ion doping.

Cantor photonic crystals are quasi-periodic and could induce an optical fractal phenomenon as the sequence number of photonic crystals increases, which is a characteristic that the periodic photonic crystals cannot possess. The optical fractal states are resonant transmission modes, of which the electric field power could be greatly confined in the defect layers of quasi-periodic photonic crystals. The values of transmittance are maximum and the reflectance values are minimum at the optical fractal states. In particular, as Cantor photonic crystals satisfy parity-time symmetry, the right and left reflection coefficients are nonreciprocal. Consequently, the right/left reflectance is zero at the optical fractal states as the gain–loss factor of materials is $q \neq 0$, while the left/right reflectance is nonzero for incident light with the same wavelength. This effect is called unidirectional invisibility. Here, we only explore the reflection nonreciprocity of light around one of the optical fractal states near the center of normalized frequency, so the unidirectional invisible effect may also exist at other fractal states and in other aperiodic photonic crystals, such as Octonacci, Thue–Morse, Rudin–Shapiro, and period-doubling photonic crystals [29–33]

3. Unidirectional Invisible Phenomenon

As transverse magnetic (TM) polarized light wave is normally incident on the PT-symmetric structure from the left, Figure 2 demonstrates the transmission spectra for a value of the gain–loss factor $q = 5$. The transverse coordinate of $(\omega - \omega_0)/\omega_{\text{gap}}$ is the normalized angular frequency, where the symbol c is the vacuum velocity of light and $\omega = 2\pi c/\lambda$, $\omega_0 = 2\pi c/\lambda_0$, and $\omega_{\text{gap}} = 4\omega_0 \arcsin |[\text{Re}(n_H) - \text{Re}(n_L)]/[\text{Re}(n_H) + \text{Re}(n_L)]|^2/\pi$ are, respectively, called the incident angular frequency of light, the central angular frequency, and the photonic bandgap. The transmission and reflection spectra are derived by the forward transmission matrix method (FTMM) [22]. The symbol T represents the transmittance, while R_f and R_b , respectively, represent the reflectance of lights incident from the left and right.

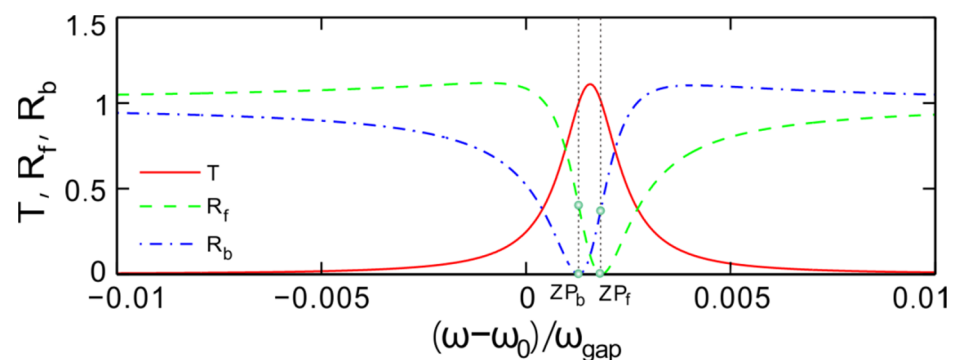


Figure 2. Transmittance and reflectance varying with the normalized frequency, respectively. Two lights are normally incident from the left and right, respectively. The gain–loss factor is $q = 5$.

The transmission spectra are coincident with each other for lights normally incident from the left and right, while the reflection spectra are not coincident. There is a peak in the transmittance curve and the peak value is $T = 1.11$ at $(\omega - \omega_0)/\omega_{\text{gap}} = 0.0016$. The peak corresponds to a resonant mode which stems from the electric field localization. The combined effect of the optical gain in materials and the mode field localization causes the peak transmittance to exceed 1.

For two lights incident from the left and right, there is a valley in each reflection spectrum. The two valleys are denoted as ZP_f and ZP_b for the two directions' incident lights, respectively. The valley of ZP_f is located at $(\omega - \omega_0)/\omega_{\text{gap}} = 0.0018$ for the left incident light, while for the right incident light the reflection valley of ZP_b is located at $(\omega - \omega_0)/\omega_{\text{gap}} = 0.0013$. One can find that the maximum transmittance is between the two reflectivity zeros.

The characteristic is that the reflection curve of the left incident light does not identify with that of the right incident light. In particular, the left incident reflectance is $R_f = 0$ at ZP_f , while the right incident reflectance is $R_b = 0.3896$. As light is incident from the left at the normalized frequency of $(\omega - \omega_0)/\omega_{\text{gap}} = 0.0018$, the reflectance is zero, *viz.* reflectionless transmission. In this case, the device is invisible to the left incident light wave, while the reflectance is nonzero and visible for a light incident from the right at the same frequency. Similarly, the right reflectance is $R_b = 0$ at ZP_b at the normalized frequency $(\omega - \omega_0)/\omega_{\text{gap}} = 0.0013$, while the left reflectance is $R_f = 0.3969$. In this case, for the frequency of $(\omega - \omega_0)/\omega_{\text{gap}} = 0.0013$, the device is invisible to the right incident light while it is visible to the left incident light. Therefore, this effect could be utilized for the unidirectionally optical invisibility of particular wavelengths.

The gain–loss factor can be positive and negative. In PT-symmetric systems, the imaginary part of the refractive index of the whole structures submits to odd symmetry $n_i(z) = -n_i(-z)$. For a specific material, the positive imaginary part of the refractive index represents loss and the negative imaginary part of the refractive index represents gain. We have only demonstrated reflectance and transmittance of light for the case of positive q , so for the case of $q < 0$, one can derive the reflection and transmission characteristic from the case of $q > 0$ by flipping the device horizontally.

As a light is normally incident from the left, Figure 3a gives the reflectance in the parameter space. The parameter space is composed of the gain–loss factor and the normalized frequency. The symbol of R_f represents the forward-incident light reflectance and $\log_{10}(R_f)$ is the logarithm of R_f . There is a groove of reflectance in the parameter space caused by modulating q and $(\omega - \omega_0)/\omega_{\text{gap}}$ simultaneously. The value on the path of the reflectance groove is zero, *viz.* the groove corresponds to the zero reflection point changing trajectory and denoted by ZP_f .

For a right incident light where the incident is $\theta = 0^\circ$, the reflectance is labeled by R_b . In the parameter space, the reflectance is a function of the gain–loss factor and the normalized frequency as shown in Figure 3b. One can see that, compared with Figure 3a, there is also a valley trajectory in the parameter space as the gain–loss factor and normalized frequency change. The minimum value of the right reflection is zero as well and denoted by ZP_b . One can find that the left and right trajectories composed of the zero-reflection points do not coincide, which manifests that the reflection is direction-dependent and nonreciprocal.

As lights are incident from the left and right, Figure 3c gives the transmittance in the parameter space. The values of transmittance are the same for the two directions' incident lights. The transmittance of light is denoted by T and there is a peak transmittance trajectory in the parameter space denoted by PT. The peak varies with the gain–loss factor and the normalized frequency. The peak value increases with the increase in the gain–loss factor and normalized frequency. In other words, the resonance of the transmission mode is improved by increasing the gain–loss factor, which results from the enhancement of the electric field localization.

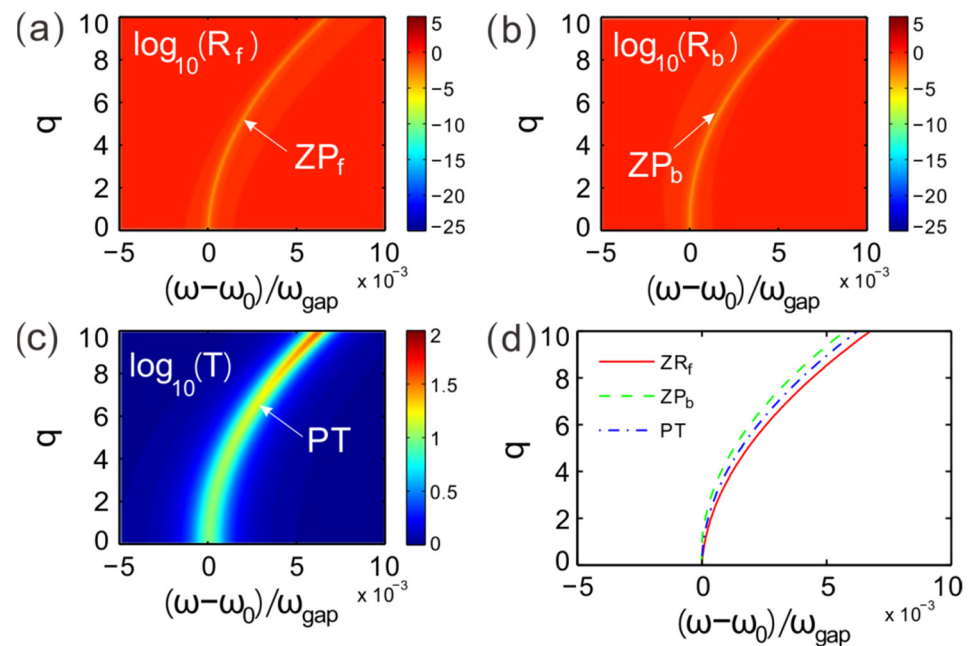


Figure 3. (a,b) Reflectance for lights incident from the left and right, respectively. (c) Transmittance of light in the parameter space. (d) Zero point of reflection and peak point varying with the normalized frequency and gain–loss factor.

Figure 3d gives the transmittance peak (PT), with the zero points of the left and right reflection (ZP_f and ZP_b) varying with the gain–loss factor. The zero points of these two direction reflection lights split as the gain–loss increases. Furthermore, as the gain–loss factor increases, the zero reflection points split more widely. The peak of transmittance is local between the left and right reflectionless points. This demonstrates that the left and right reflection nonreciprocity phenomenon is more obvious for a greater gain–loss factor. Otherwise, zero points of reflection splitting induce the localization enhancement of the electric field and resonance of the transmission mode.

For a light incident from the left, there are a series of zero-points of reflectance in the parameter space. We have denoted the zero-point by ZP_f which is local at $[q, (\omega_{fz} - \omega_0)/\omega_{\text{gap}}]$. For each fixed value of the gain–loss factor, there is a corresponding left reflectionless point. Meanwhile, this normalized frequency corresponds to a specific wavelength, so we can denote the reflectionless point by $[q, \lambda_{fz}]$. The zero-point of reflection changes with the gain–loss factor; therefore, the corresponding wavelength of the reflectionless point changes as well. For a given q , the reflectance is $R_f = 0$ as the incident light wavelength is $\lambda = \lambda_{fz}$. Therefore, people cannot sense the existence of the photonic crystal, and the photonic device is left invisible to this left incident particular wavelength. Keeping the gain–loss factor unchanged, the reflectance is $R_b > 0$ for the right incident light. For a given value of q , the right reflectance of λ_{fz} (the left reflectionless incident wavelength) varies with the gain–loss factor, as shown in Figure 4a. As the gain–loss factor increases, this modulates the incident wavelength to leave the left reflectance containing zero unchanged, while the right reflectance keeps increasing at the same incident wavelength. Therefore, the device is unidirectionally invisible for the left incident light and visible for the right incident light.

Figure 4b gives the left reflectionless wavelength varying with the gain–loss factor. The corresponding wavelength is $\lambda_{fz} = 1.55 \mu\text{m}$ for $q = 0$ and the corresponding wavelength is $\lambda_{fz} = 1.5436 \mu\text{m}$ for $q = 10$. The left incident invisibility wavelength decreases with the increase in the gain–loss factor. Here, we investigate the reflectionless points in the non-reciprocal left and right reflection spectra of lights. This effect is called unidirectional invisibility and could be utilized for unidirectional invisibility for a given gain–loss factor $q = 10$, the reflectance $R_f = 0$ as a light is incident from the left with a wavelength of $\lambda_{fz} = 1.5436 \mu\text{m}$, while the right reflectance is $R_b \neq 0$ with the same incident wave-

length. Therefore, this photonic device is invisible for the left incident probing wave of $\lambda_{fz} = 1.5436 \mu\text{m}$ and visible for the same right incident probing wave, as the gain–loss factor is $q = 10$.

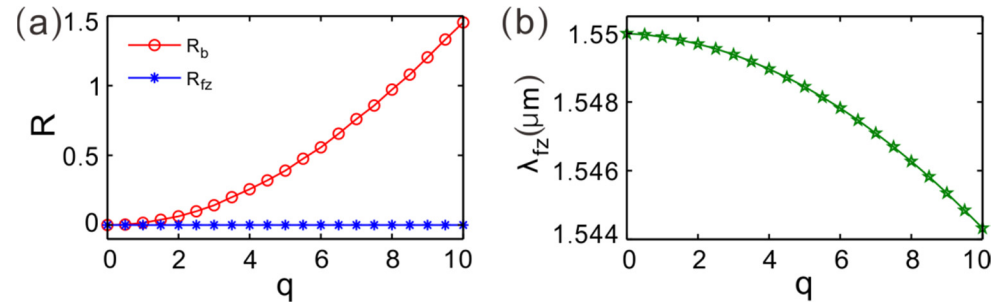


Figure 4. (a) The right reflectance varying with the gain–loss factor at the left-reflectionless incident wavelength. (b) The left unidirectionally invisible wavelength changing with the gain–loss factor.

The zero reflection of the right incident light is denoted by $[q, \lambda_{bz}]$. In the same way, for a fixed q the left reflectance is nonzero as the light impinges upon the structure normally from the right in the corresponding wavelength of λ_{bz} , meaning that the device can be unidirectionally invisible for the right incident light. The left reflectance at the wavelength of the right reflectionless varies with the gain–loss factor, as shown in Figure 5a. By modulating the incident wavelength, the right reflectance contains $R_{bz} = 0$ as the gain–loss factor increases. Meanwhile, the reflectance of the left incident light increases with the increase in the gain–loss factor. Therefore, the device is invisible for the right incident light, while it is visible for the left incident light.

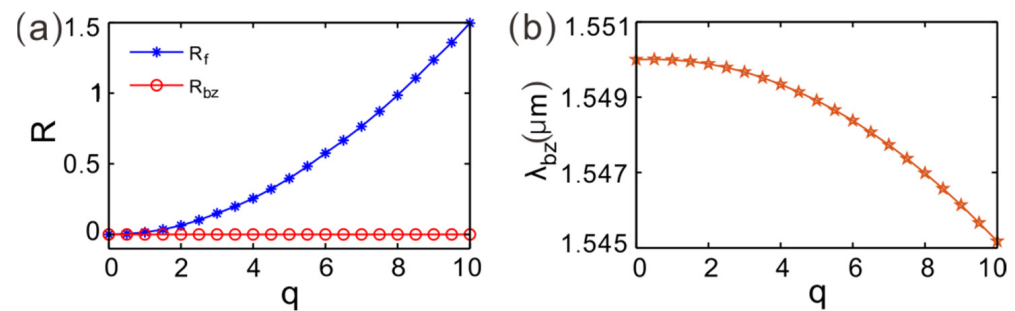


Figure 5. (a) Left reflectance varying with the gain–loss factor at the right-reflectionless incident wavelength. (b) Right unidirectionally invisible wavelength changing with the gain–loss factor.

Figure 5b provides the corresponding wavelength of the right reflectionless changing with the gain–loss factor. The invisibility wavelength is $\lambda_{bz} = 1.55 \mu\text{m}$ for $q = 0$ and the corresponding wavelength is $\lambda_{bz} = 1.5478 \mu\text{m}$ for $q = 10$. The right incident invisibility wavelength decreases with the increase in the gain–loss factor as well.

For 1D photonic crystals with regular geometric structures, the transmittance and reflectance of plane waves are submitted to the exact mathematical expressions in TMM. Here, we choose some parameters to verify this conclusion. For a nonzero value of the gain–loss factor $q = 5$, *viz.* $n_H = 3.53 + 0.05i$, $n_{H'} = 3.53 - 0.05i$, $n_L = 1.46 + 0.05i$, and $n_{L'} = 1.46 - 0.05i$, Figure 6a gives the transmission spectra of lights derived by two different simulating methods of TMM and (finite difference time domain) FDTD. One can see that the two simulating results are demonstrated to be coincident with each other. There is a peak in the transmittance curve and the corresponding wave of the transmission peak is $\lambda = 1.5487 \mu\text{m}$. For the transmission mode, Figure 6b,c provide the distribution of the electric field in TMM and FDTD, respectively. The electric field power is mainly restricted around the center defect layers and the results simulated in two different methods are coincident.

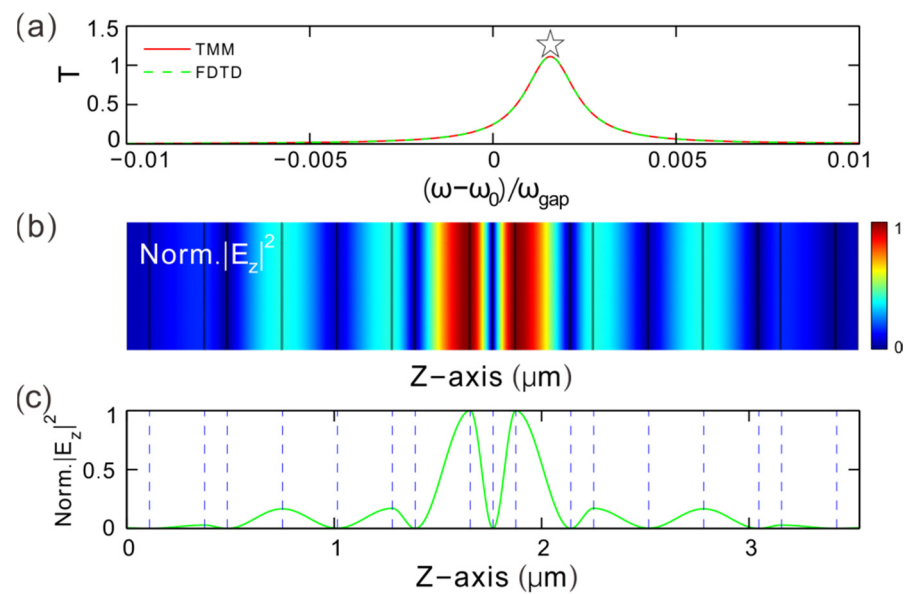


Figure 6. (a) Transmission spectra for the normally incident light waves for $q = 5$ in two different simulating methods. (b,c) Electric field distribution of the transmission mode simulated by TMM and FDTD, respectively.

The dielectric slabs of 1D photonic crystals are arranged along the Z-axis and the whole thickness of this structure is $3.5323 \mu\text{m}$ in the horizontal direction. More practical 2D and 3D structures can be constructed, since the size of 1D photonic crystals in the X-axis or Y-axis is approximately two orders of magnitude larger than that in the Z-axis.

For a given value of q , there is a corresponding wavelength at which the reflectance is zero as the light is incident from the left, while the right reflectance is nonzero at the same incident wavelength. Similarly, for a light with some other wavelengths, the right reflectance is zero while the left reflectance is nonzero. This effect can be utilized for optical unidirectionally invisibility. The invisibility wavelength could be tuned by the gain–loss factor flexibly.

4. Conclusions

In conclusion, the reflectionless effect and the dependence of reflection on direction are investigated in PT-symmetric Cantor photonic crystals. Two dielectrics subject to the Cantor sequence array along the Z-axis and their refractive indices are modulated to satisfy PT symmetry. The Cantor photonic crystals support optical fractal states which are resonant states. The left and right reflectionless states are local at around the resonant mode. The PT symmetry leads to the unidirectional invisibility of light. By modulating the gain–loss factor, PT symmetry could further improve the resonance of an optical fractal state. Subsequently, the left and right zero points of reflection are split by tuning the gain–loss factor of materials. In particular, the unidirectionally invisible wavelength changes with the gain–loss factor. This study could have applications for optical reflectors and invisible cloaks, such as spatially tunable modern lasers [34], wavelength splitters [35], dispersion-controlled optical group delay devices [36], multichannel multiplexors [37], and rendering objects undetectable [38,39].

Author Contributions: Conceptualization, M.W., F.L. and Y.W.; funding acquisition, M.W., F.L. and D.Z.; software, M.W., F.L. and D.Z.; investigation, M.W., F.L. and Y.W.; writing—original draft preparation, M.W.; writing—review and editing, F.L., D.Z. and Y.W.; supervision, Y.W.; project administration, Y.W. All authors have read and agreed to the published version of the manuscript.

Funding: The Scientific Research Project of Hubei University of Science and Technology (2021-22X21, BK2020171); the Science and Technology Plan Research Project of Hubei Education Department (B2020155); the Co-operative Education Reform Project Innovative Undertaking Together with the Education Ministry for China (201901033016).

Institutional Review Board Statement: Not applicable.

Informed Consent Statement: Not applicable.

Data Availability Statement: Not applicable.

Conflicts of Interest: The authors declare no conflict of interest.

References

1. Amoosoltani, N.; Mehrabi, K.; Zarifkar, A.; Farmani, A.; Yasrebi, N. Double-ring resonator plasmonic refractive index sensor utilizing dual-band unidirectional reflectionless propagation effect. *Plasmonics* **2021**, *16*, 1277–1285. [[CrossRef](#)]
2. Lee, J.; Lee, J. Generic and versatile reflectionless filter topology and its applications to distributed-element reflectionless bandpass filters. *IEEE Trans. Microw. Theory Tech.* **2021**, *69*, 3058–3069. [[CrossRef](#)]
3. Gu, X.; Bai, R.; Zhang, C.; Jin, X.R.; Zhang, Y.Q.; Zhang, S.; Lee, Y. Unidirectional reflectionless propagation in a non-ideal parity-time metasurface based on far field coupling. *Opt. Express* **2017**, *25*, 11778–11787. [[CrossRef](#)] [[PubMed](#)]
4. Rahm, M.; Cummer, S.A.; Schurig, D.; Pendry, J.B.; Smith, D.R. Optical design of reflectionless complex media by finite embedded coordinate transformations. *Phys. Rev. Lett.* **2008**, *100*, 063903. [[CrossRef](#)] [[PubMed](#)]
5. Feng, L.; Xu, Y.-L.; Fegadolli, W.S.; Lu, M.-H.; Oliveira, J.; Almeida, V.R.; Chen, Y.-F.; Scherer, A. Experimental demonstration of a unidirectional reflectionless parity-time metamaterial at optical frequencies. *Nat. Mater.* **2013**, *12*, 108–113. [[CrossRef](#)] [[PubMed](#)]
6. Klotz, G.; Malléjac, N.; Guenneau, S.; Enoch, S. Controlling frequency dispersion in electromagnetic invisibility cloaks. *Sci. Rep.* **2019**, *9*, 6022. [[CrossRef](#)]
7. Renger, J.; Kadic, M.; Dupont, G.; Aimovi, S.S.; Enoch, S. Hidden progress: Broadband plasmonic invisibility. *Opt. Express* **2010**, *18*, 15757–15768. [[CrossRef](#)]
8. El-Ganainy, R.; Khajavikhan, M.; Christodoulides, D.N.; Ozdemir, S.K. The dawn of non-Hermitian optics. *Commun. Phys.* **2019**, *2*, 37. [[CrossRef](#)]
9. Ye, Z.; Yang, M.; Zhu, L.; Chen, P.Y. PTX-symmetric metasurfaces for sensing applications. *Front. Optoelectron.* **2021**, *14*, 211–220. [[CrossRef](#)]
10. Cao, Y.; Fu, Y.; Zhou, Q.; Xu, Y.; Gao, L.; Chen, H. Giant Goos-Hänchen shift induced by bounded states in optical PT-symmetric bilayer structures. *Opt. Express* **2019**, *27*, 7857. [[CrossRef](#)]
11. Ge, L.; Chong, Y.D.; Stone, A.D. Conservation relations and anisotropic transmission resonances in one-dimensional PT-symmetric photonic heterostructures. *Phys. Rev. A* **2012**, *85*, 445–457. [[CrossRef](#)]
12. Bender, C.M.; Boettcher, S. Real spectra in non-Hermitian Hamiltonians having PT symmetry. *Phys. Rev. Lett.* **1998**, *80*, 5243–5246. [[CrossRef](#)]
13. Sarisaman, M.; Tas, M. PT-symmetric coherent perfect absorber with graphene. *J. Opt. Soc. Am. B* **2018**, *35*, 2423–2432. [[CrossRef](#)]
14. Wang, H.; Kong, W.; Zhang, P.; Li, Z.; Zhong, D. Coherent perfect absorption laser points in one-dimensional anti-parity-time-symmetric photonic crystals. *Appl. Sci.* **2019**, *9*, 2738. [[CrossRef](#)]
15. Kirikchi, O.B.; Karjanto, N. Discrete solitons dynamics in PT-symmetric oligomers with complex-valued couplings. *Nonlinear Dynamics* **2021**, *103*, 2769–2782. [[CrossRef](#)]
16. Zhao, D.; Ke, S.; Hu, Y.; Wang, B.; Lu, P. Optical bistability of graphene embedded in parity-time-symmetric photonic lattices. *J. Opt. Soc. Am. B* **2019**, *36*, 1731. [[CrossRef](#)]
17. Zhao, D.; Xu, B.; Guo, H.; Xu, W.; Zhong, D.; Ke, S. Low threshold optical bistability in aperiodic PT-symmetric lattices composited with Fibonacci sequence dielectrics and graphene. *Appl. Sci.* **2019**, *9*, 5125. [[CrossRef](#)]
18. Xu, X.; Shi, L.; Ren, L.; Zhang, X. Optical gradient forces in PT-symmetric coupled-waveguide structures. *Opt. Express* **2018**, *26*, 10220–10229. [[CrossRef](#)]
19. Yuce, C.; Oztas, Z. PT symmetry protected non-Hermitian topological systems. *Sci. Rep.* **2018**, *8*, 17416. [[CrossRef](#)]
20. Bergman, A.; Duggan, R.; Sharma, K.; Tur, M.; Alù, A. Observation of anti-parity-time-symmetry, phase transitions and exceptional points in an optical fibre. *Nat. Commun.* **2021**, *12*, 486.
21. Liu, Q.; Liu, J.; Zhao, D.; Wang, B. On-chip experiment for chiral mode transfer without enclosing an exceptional point. *Phys. Rev. A* **2021**, *103*, 023531. [[CrossRef](#)]
22. Lin, Z.; Ke, S.; Zhu, X.; Li, X. Square-root non-Bloch topological insulators in non-Hermitian ring resonators. *Opt. Express* **2021**, *29*, 8462–8476. [[CrossRef](#)] [[PubMed](#)]
23. Wang, Q.; Wang, X.; Zhang, L.; Wang, Y. Tunable defect modes of one-dimensional photonic crystals containing a Dirac semimetal-based metamaterial defect layer. *Appl. Opt.* **2019**, *58*, 94–101. [[CrossRef](#)] [[PubMed](#)]
24. Zhang, Z.R.; Li, H.Q.; Chen, H.; Hu, C.L.; Zhou, P. Coherent perfect absorption in one-dimensional photonic crystal with a PT-symmetric defect. *Europhys. Lett.* **2014**, *105*, 107–110. [[CrossRef](#)]

25. Ding, K.; Zhang, Z.Q.; Chan, C.T. Coalescence of exceptional points and phase diagrams for one-dimensional PT-symmetric photonic crystals. *Phys. Rev. B* **2015**, *92*, 235310. [[CrossRef](#)]
26. Trevino, J.; Seng, F.L.; Noh, H.; Cao, H.; Negro, L.D. Geometrical structure, multifractal spectra and localized optical modes of aperiodic Vogel spirals. *Opt. Express* **2012**, *20*, 3015–3033. [[CrossRef](#)]
27. Davydova, M.G.; Korolenko, P.V.; Ryzhikov, S.B.; Ryzhikova, Y.V. Pattern analysis of fractal properties in multilayer systems with metamaterials. *Phys. Wave Phenom.* **2016**, *24*, 17–21. [[CrossRef](#)]
28. Nicola, S.D. Reflection and transmission of cantor fractal layers. *Opt. Commun.* **1994**, *111*, 11–17. [[CrossRef](#)]
29. Yu, Y.; Da, H. Broadband and perfect absorption of monolayer MoS₂ with Octonacci quasi-photonic crystal. *Phys. B Condens. Matter* **2020**, *604*, 412684. [[CrossRef](#)]
30. Ni, H.; Wang, J.; Wu, A. Optical bistability in aperiodic multilayer composed of graphene and Thue-Morse lattices. *Optik* **2021**, *242*, 167163. [[CrossRef](#)]
31. Wang, L.; Liu, F.; Liu, F.; Qin, Z.; Zhang, Y.; Zhong, D.; Ni, H. Optical fractal and exceptional points in pt symmetry Thue-Morse photonic multilayers. *Opt. Mater.* **2021**, *123*, 111821. [[CrossRef](#)]
32. Rahimi, H. Analysis of photonic spectra in Thue-Morse, double-period and Rudin-Shapiro quasiregular structures made of high temperature superconductors in visible range. *Opt. Mater.* **2016**, *57*, 264–271. [[CrossRef](#)]
33. Fang, Y.T.; Liang, Z.C. Unusual transmission through usual one-dimensional photonic crystal in the presence of evanescent wave. *Opt. Commun.* **2010**, *283*, 2102–2108. [[CrossRef](#)]
34. Huang, Y.; Ying, Z.; Wu, S. Spatially tunable laser emission in dye-doped photonic liquid crystals. *Appl. Phys. Lett.* **2006**, *88*, 011107. [[CrossRef](#)]
35. Gerken, M.; Miller, D. Relationship between the superprism effect in one-dimensional photonic crystals and spatial dispersion in nonperiodic thin-film stacks. *Opt. Lett.* **2005**, *30*, 2475. [[CrossRef](#)]
36. Mori, D.; Baba, T. Dispersion-controlled optical group delay device by chirped photonic crystal waveguides. *Appl. Phys. Lett.* **2004**, *85*, 1101–1103. [[CrossRef](#)]
37. Jonsson, F.; Flytzanis, C. Spectral windowing with chirped magneto-optical bragg gratings. *J. Opt. Soc. Am. B* **2005**, *22*, 293–298. [[CrossRef](#)]
38. Farhat, M.; Chen, P.; Guenneau, S.; Enoch, S.; McPhedran, R.; Rockstuhl, C.; Lederer, F. Understanding the functionality of an array of invisibility cloaks. *Phys. Rev. B* **2011**, *84*, 235105. [[CrossRef](#)]
39. Hui, F.M.; Cui, T.J. Three-dimensional broadband ground-plane cloak made of metamaterials. *Nat. Commun.* **2010**, *1*, 21.